International Journal of Pharmaceutics: X 5 (2023) 100142

Contents lists available at ScienceDirect

International Journal of Pharmaceutics: X

journal homepage: www.sciencedirect.com/journal/international-journal-of-pharmaceutics-x

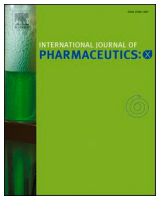

Development of 3D-printed vaginal devices containing metronidazole for alternative bacterial vaginosis treatment

Emilia Utomo [1], Juan Domínguez-Robles [1,*], Qonita Kurnia Anjani, Camila J. Picco, Anna Korelidou, Erin Magee, Ryan F. Donnelly, Eneko Larrañeta [*]

School of Pharmacy, Queen's University Belfast, Medical Biology Centre, 97 Lisburn Road, Belfast BT9 7BL, UK

ARTICLE INFO

Keywords:
3D printing
Intravaginal devices
Mucoadhesive devices
Metronidazole
Bacterial vaginosis

ABSTRACT

Bacterial vaginosis (BV) is an abnormal condition caused by the change of microbiota in the vagina. One of the most common bacteria found in the case of BV is *Gardnerella vaginalis*, which is categorised as anaerobic facultative bacteria. Currently, the available treatment for BV is the use of antibiotics, such as metronidazole (MTZ), in topical and oral dosage forms. The limitation of the currently available treatment is that multiple administration is required and thus, the patient needs to apply the drug frequently to maintain the drug efficacy. To address these limitations, this research proposed prolonged delivery of MTZ in the form of intravaginal devices made from biodegradable and biocompatible polymers. Semi-solid extrusion (SSE) 3D printing was used to prepare the intravaginal devices. The ratio of high and low molecular weight poly(caprolactone) (PCL) was varied to evaluate the effect of polymer composition on the drug release. The versatility of SSE 3D printer was used to print the intravaginal devices into two different shapes (meshes and discs) and containing two different polymer layers made from PCL and a copolymer of methyl vinyl ether and maleic anhydride (Gantrez™-AN119), which provided mucoadhesive properties. Indeed, this layer made from Gantrez™-AN119 increased *ca.* 5 times the mucoadhesive properties of the final 3D-printed devices (from 0.52 to 2.57 N). Furthermore, MTZ was homogenously dispersed within the polymer matrix as evidenced by scanning electron microscopy analysis. Additionally, *in vitro* drug release, and antibacterial activity of the MTZ-loaded intravaginal devices were evaluated. Disc formulations were able to sustain the release of MTZ for 72 h for formulations containing 70/30 and 60/40 ratio of high molecular weight/low molecular weight PCL. On the other hand, the discs containing a 50/50 ratio of high molecular weight/low molecular weight PCL showed up to 9 days of release. However, no significant differences in the MTZ release from the MTZ-loaded meshes (60/40 and 50/50 ratio of high molecular weight/low molecular weight PCL) were found after 24 h. The results showed that the different ratios of high and low molecular weight PCL did not significantly affect the MTZ release. However, the shape of the devices did influence the release of MTZ, showing that larger surface area of the meshes provided a faster MTZ release. Moreover, MTZ loaded 3D-printed discs (5% *w*/w) were capable of inhibiting the growth of *Gardnerella vaginalis*. These materials showed clear antimicrobial properties, exhibiting a zone of inhibition of 19.0 ± 1.3 mm. Based on these findings, the manufactured represent a valuable alternative approach to the current available treatment, as they were able to provide sustained release of MTZ, reducing the frequency of administration and thus improving patient compliance.

1. Introduction

Bacterial vaginosis (BV) is one of the most common pathologic conditions that occur in women during the reproductive age (Redelinghuys et al., 2020). This condition is caused by a change in vaginal microbiota from lactobacilli to facultative anaerobic bacteria (Muzny and Kardas, 2020). Vaginal flora is usually predominated by the "healthy" Lactobacilli species, but when diverse bacteria from other taxonomic groups, including *Gardnerella*, *Bacteroides* and *Anaerococcus*, among others, begin to overgrow and become dominant, BV can result.

* Corresponding authors.
E-mail addresses: j.dominguezrobles@qub.ac.uk (J. Domínguez-Robles), e.larraneta@qub.ac.uk (E. Larrañeta).
[1] These authors contributed equally to this work. Joint First Authors: Emilia Utomo and Juan Domínguez-Robles.

https://doi.org/10.1016/j.ijpx.2022.100142
Received 14 September 2022; Received in revised form 5 December 2022; Accepted 5 December 2022
Available online 6 December 2022

Therefore, BV is cause by disruption to the microbiota homeostasis caused by an imbalance in the vaginal flora that has been associated with a wide variety of adverse health outcomes (Morrill et al., 2020). The current treatment for BV includes the use of oral and vaginal antibiotics. Metronidazole (MTZ) is one of the most widely used antibiotics to treat BV and the length of treatment is usually between 5 and 7 days (Anjani et al., 2022; Jones, 2019; Sweetman, 2009). MTZ is available in oral and vaginal gel dosage forms (Chavoustie et al., 2015; Goje et al., 2021; Löfmark et al., 2010; Verwijs et al., 2020). However, oral administration would experience first-pass metabolism and can cause gastrointestinal adverse effects (Herman and Santos, 2022). In addition, it has been reported that the effect of intravaginal administration of MTZ was as effective as oral administration but with less gastrointestinal issues (Hanson et al., 2001; Mitchell et al., 2009; Sweetman, 2009). Accordingly, local administration of MTZ is preferred to provide direct action to the target site. Unfortunately, the current available MTZ vaginal gel dosage forms have several disadvantages such as frequent daily application and the possibility of the gel being rinsed by the vaginal fluid (Patil et al., 2019). Thus, 3D- printed MTZ-loaded vaginal devices are proposed as an alternative delivery system approach for BV treatment.

3D-printing is an emerging technology, which has been explored in the manufacturing of pharmaceutical devices (Ali et al., 2020; Awad et al., 2019; Dominguez-Robles et al., 2019; Domínguez-Robles et al., 2022; Goyanes et al., 2015; Khaled et al., 2018b; Martinez et al., 2018; Mathew et al., 2019; Robles-Martinez et al., 2019; Seoane-Viaño et al., 2021; Trenfield et al., 2018). Numerous vaginal devices have been developed by using Fused Deposition Modeling (FDM), one of the most popular 3D printing technologies (Arany et al., 2021; Domínguez-Robles et al., 2020; Farmer et al., 2020, 2021). In this study, a different technology, namely semi-solid extrusion (SSE) was employed to successfully prepare the 3D-printed intravaginal devices. This technology uses the aid of heat and mechanical pressure to extrude the materials comprising the polymer and the drug (El Aita et al., 2020; Mohammed et al., 2021; Seoane-Viaño et al., 2021). The advantage of using this method is the ability to alter the formulation in small scale (Yan et al., 2020). Hence, this method is promising for the fabrication of individualized dose in hospital (Seoane-Viaño et al., 2021).

In this paper, 3D-printed intravaginal devices containing MTZ were prepared in two different shapes, namely meshes and discs using poly (caprolactone) (PCL), a biodegradable and biocompatible polymer (Korelidou et al., 2022; Stewart et al., 2018, 2021; Utomo et al., 2022). The combination of high and low molecular weight PCL has been proven by previous studies to produce the most desirable properties of 3D-printed devices (Domínguez-Robles et al., 2021a, 2021b). The objective of this research was to develop intravaginal devices to provide prolonged release of MTZ for BV treatment. In brief, MTZ vaginal devices were prepared by using different ratios of high and low molecular weight PCL by using a 3D bioprinter (SSE technology). Furthermore, an additional layer containing Gantrez™-AN119 was added on the top of the 3D-printed intravaginal devices to provide mucoadhesive properties (Irache et al., 2005). The resulting 3D-printed devices were characterized using different techniques to evaluate their physicochemical properties. Moreover, MTZ release kinetics, mucoadhesive properties and antimicrobial activity were evaluated.

2. Materials and methods

2.1. Materials

MTZ was purchased from Tokyo Chemical Industry, Tokyo, Japan. PCL 6506 (Mw = 50,000 Da) henceforth referred to as H-PCL and PCL 2054 (Mw = 550 Da) henceforth referred to as L-PCL were kindly provided by Perstop (Malmö, Sweden). Gantrez™-AN119, a copolymer of methyl vinyl ether and maleic anhydride, was a gift from Ashland, (Kidderminster, UK). Porcine mucin was obtained from Sigma Aldrich (Dorset, UK). Microcrystalline cellulose (MCC), Avicel PH 102, was acquired by IMCD UK Limited (Sutton, UK). *Gardnerella vaginalis* NCTC 10287 was incubated anaerobically on brain heart infusion (BHI) broth at 37 °C in for 48–72 h to perform the disk diffusion test. All the chemicals used were of pharmaceutical grade.

2.2. Preparation of 3D printed intravaginal devices containing MTZ

The formulations of vaginal devices were comprised of the mixture of H-PCL and L-PCL in different ratios and 5% (*w*/w) of MTZ, as presented in Table 1. Initially, MTZ was grinded using a mortar and pestle to reduce the particle size. Subsequently, MTZ was mixed with L-PCL using a SpeedMixer™ DAC 150.1 FVZ-K (Hauschild GmbH & Co. KG, Westfalen, Germany) at 3500 rpm for 3 min. A weighed amount of H-PCL was then added and mixed using the SpeedMixer™ DAC 150.1 FVZ-K at 3500 rpm for 5 min to obtain a homogenous mixture. Afterwards, the final mixture was placed into a metal syringe of the 3D bioprinter equipped with 0.5 mm nozzle. The design of both vaginal meshes and discs was performed using a computer-aided design (CAD) software, which was further printed using a 3D bioprinter (Bioscaffolder 3.2., GeSiM) (Radeberg, Germany). The diameter of both meshes and discs was 13 mm. Moreover, meshes had a weight which ranged from 48.2 to 59.4 mg, while discs had a weight, which ranged from 83.9 to 109.6 mg. The printer was set with the print speed of 10 mm/s and temperature of 60 °C. The strand height and width were 0.25 and 0.50 mm, respectively. Finally, the strand distance was set at 1.6 and 0.65 mm for meshes and discs, respectively. Both devices, meshes and discs were composed of 2 layers of extruded materials.

The additional mucoadhesive layer of the intravaginal devices was added using a different type of cartridge but from the same 3D bioprinter. In this case, instead of using temperature and mechanical force, air pressure was employed to 3D print the mucoadhesive layer. Gantrez™ AN-119 was used as the mucoadhesive polymer, which was firstly dissolved in acetone to obtain a concentration of 40% *w*/*v*. The obtained solution was subsequently placed in a new cartridge equipped with 0.4 mm nozzle. The printer speed was set at 30 mm/s and the employed pressure was 60 kPa. The strand width and height were both 0.410 mm while the strand distance was 1.8 mm. The mucoadhesive part, which consisted of 1 layer of Gantrez™ AN-119, was printed on each of MTZ-loaded vaginal discs (F1C-M). Afterwards, the mucoadhesive layer was dried at room temperature for 24 h to allow the evaporation of acetone. The final 3D-printed intravaginal devices, containing the mucoadhesive layer were stored at room temperature for further evaluation.

2.3. Physicochemical characterisation

The surface of the 3D printed intravaginal devices was assessed using a scanning electron microscope (SEM) (Tabletop Microscope® TM 3030). Evaluated samples were taken before and after the release study. Moreover, the thickness of both the PCL-based part and the mucoadhesive layer of the 3D-printed intravaginal device were measured by using optical coherence tomography (OCT).

Thermal properties of MTZ-loaded 3D-printed materials and pure compounds were evaluated using differential scanning calorimetry (DSC) and thermogravimetric analysis (TGA). DSC analysis was performed to observe the melting point and crystallinity of materials. For this purpose, samples between 5 and 10 mg were heated in a sealed

Table 1
Composition of MTZ-loaded intravaginal devices.

Formulations	H-PCL (%w/w)	L-PCL (%w/w)	MTZ (% w/w)	H-PCL/L-PCL Ratio
F1	66.5	28.5	5.0	70/30
F2	57.0	38.0	5.0	60/40
F3	47.5	47.5	5.0	50/50

aluminum pan from 25 to 200 °C at a rate of 10 °C/min using a DSC Q20 (TA Instruments, New Castle, USA). Moreover, TGA analysis was performed to determine the degradation of samples caused by increasing temperature. For this purpose, once again samples between 5 and 10 mg were heated from room temperature to 500 °C at a rate of 10 °C/min using a TGA Q50 (TA Instruments, New Castle, USA). Data analysis was done using TA Universal Analysis software (TA Instruments, New Castle, USA).

Fourier transform infrared (FTIR) Accutrac FT/IR-4100 series (Jasco, Essex, UK) was used to observe chemical interactions between the different compounds of the formulations. This instrument was equipped with MIRacle™ diamond attenuated total reflection (ATR). The IR transmission spectra were recorded between 600 and 4000 cm^{-1} using 32 scans with a resolution of 4.0 cm^{-1} at room temperature.

To further evaluate the crystallinity of the 3D-printed samples, X-ray diffractometer (XRD) analysis was performed. Measurements were performed using MiniFlex II Desktop Powder X-ray Diffractometer (Rigaku Corporation, Kent, UK) equipped with Cu K_β radiation ($\lambda = 1.39$ Å). The experiment measurements were conducted at room temperature, with a voltage of 30 kV and a current of 15 mA. All samples were scanned for 2.0°/min with an angular range of 5–30° 2θ (2 theta) in continuous mode with a sampling width of 0.03°.

The drug content of the devices was determined by dissolving a small piece of MTZ-loaded disc in the mixture of acetonitrile (ACN) (1 mL) and dichloromethane (1 mL). Subsequently, 10 µL of the solution was diluted with ACN up to 1 mL. Furthermore, 100 µL of this solution was added to 900 µL of simulated vaginal fluid (SVF). To prepare SVF, 0.525 g of sodium chloride, 0.061 g of lactic acid and 0.079 g of acetic acid were weighed and added in a 100-mL volumetric flask followed by distilled water (pH 7) (Rastogi et al., 2016). The final solution was then analysed using a validated HPLC analytical method. The drug content (% drug content) was calculated using Eq. (1).

$$\%Drug\ content = \frac{C.f.V}{1000.W} x100 \quad (1)$$

Where C is the concentration measured (µg/mL), f is the dilution factor, V is the volume of the initial solution (mL) and W is the weight of MTZ disc (mg).

2.4. In vitro release studies

SVF was used as the release medium to mimic the vaginal environment. Regardless of the 3D-printed shape, both meshes and discs were placed in 5 mL of SVF at 37 °C and shaken at 40 rpm. At the specified time points, 500 µL of the release medium was taken and replaced with an equal volume of SVF to maintain the sink conditions. Samples were analysed using a validated HPLC method. Moreover, where necessary, samples were diluted to obtain a concentration in the range of the calibration curve. The percentage of drug released was calculated using Eq. (2).

$$\%Drug\ released = \frac{(x.f_d.V) + f_c}{W} x100 \quad (2)$$

Where x is the concentration measured, f_d is dilution factor, V is the volume of sample (0.5 mL), f_c is correction factor, and W is the amount of MTZ-loaded vaginal devices.

2.5. Mucoadhesion test

The mucoadhesive properties of the MTZ-loaded intravaginal devices were evaluated using TA-XT2 Texture Analyzer (Stable Microsystems, Surrey, England) as previously described by Andrews, et al. with some modifications (Andrews et al., 2009). Briefly, a mixture of porcine mucin (90% *w*/w) and MCC (10% w/w) was homogeneously mixed by vortexing. Then, 250 mg of this mixture was compressed with 10 tons of force for 30 s to obtain mucin discs with a diameter of 1.3 cm. The use of MCC prevented the mucin discs being broken during the test (data not shown). The disc was subsequently attached to the surface of the texture analyzer platform using a strong glue. Then, 50 µL of mucin solution (5% w/w) was placed on the surface of both the 3D-printed devices and mucin discs for 30 s (the excess mucin solution was removed after this time). The 3D-printed device was previously affixed to the bottom side of the inert vertical probe with the mucoadhesive layer facing downwards. The vaginal device was brought into contact with the mucin disc with a force of 1 N for 30 s to ensure intimate contact between the disc and the mucoadhesive layer. The probe was subsequently elevated at a speed of 1.0 mm/s and the force required to detach the device from the mucin disc was recorded and determined as the mucoadhesive strength (Andrews et al., 2009).

2.6. Antimicrobial activity test

3D-printed discs of F1 containing 5% (*w*/w) of MTZ were tested for the inhibitory effect on bacterial cultures of *Gardnerella vaginalis* NCTC 10287. *Gardnerella vaginalis* is an anaerobic bacterium that resides in the normal vaginal flora. For this purpose, *G. vaginalis* was incubated anaerobically in BHI broth at 37 °C for 48–72 h and 100 µL of this culture was then poured and plated on the BHI agar plate by using a cotton swab in order to obtain a bacterial lawn. 3D-printed discs were then placed on the top of the BHI agar plates and incubated anaerobically for 24 h at 37 °C. The inhibition zone diameters were measured in mm. Moreover, inoculated plates with *G. vaginalis* alone and containing PCL-based 3D-printed discs with no MTZ were also incubated at the same conditions as positive and negative controls, respectively.

2.7. Instrumentation and chromatographic condition for MTZ quantification method

MTZ quantification was performed using Reversed-Phase High Performance Liquid Chromatography (RP-HPLC). A Phenomenex® SphereClone™ C_{18} ODS (150 mm length x 4.60 mm internal diameter, 5 µm particle size) column was used as the stationary phase. The mobile phase was consisted of 0.5% *v*/v of Triethylamine (TEA) in water (pH 6.80 adjusted using phosphoric acid) as aqueous phase and methanol as organic phase with the ratio of 60:40% v/v. The injection volume was 20 µL and the flow rate was 1.0 mL/min. The wavelength of UV detection was set at 322 nm. The measurement was carried out at 25 °C. The chromatograms obtained were analysed using Agilent ChemStation® Software B.02.01.

2.8. Similarity and difference factors

The *in vitro* release profiles of each formulation were compared based on the values of the difference (f_1) and similarity (f_2) factors (Diaz et al., 2016; Larrañeta et al., 2014; Muselík et al., 2021). The value of f_1 was calculated using Eq. (3) and used to measure the percentage of difference and percent error between two release profiles at each time point. Moreover, the value of f_2 was calculated using Eq. (4) and is a logarithmic square-root transformation of differences between test and reference products over all time points.

$$f_1 = \left\{ \left[\sum_{t=1}^{n} |R_t - T_t| \right] \Big/ \left[\sum_{t=1}^{n} R_t \right] \right\} x100 \quad (3)$$

$$f_2 = 50 x log \left\{ \left[1 + (1/n) \sum_{t=1}^{n} (R_t - T_t)^2 \right]^{-0.5} x100 \right\} \quad (4)$$

Where, n is the number of sampling time, R_t is the percentage of the drug released from the reference formulation at time t, and T_t is the percentage of the drug released from the test formulation at time t. Both release profiles are considered similar when the value of f_1 is between

0 and 15 and f_2 is between 50 and 100.

2.9. Statistical analysis

Statistical analysis was performed using GraphPad Prism® version 8.0 (GraphPad Software, San Diego, California, USA). The normality of data distribution was assessed using the Shapiro-Wilk test, with a p-value of >0.05 indicating that the data were normally distributed. Data were expressed as a mean ± standard deviation and compared using one-way analysis of variance (ANOVA) with Tukey's post-hoc. Additionally, independent t-test was applied for the analysis between two groups. In all cases, p-value <0.05 indicated a statistically significant difference between tested groups.

3. Results and discussion

3.1. Preparation of 3D printed vaginal devices containing MTZ

The intravaginal devices were successfully printed using SSE 3D printing technology. Two different shapes - meshes and discs, and two different conditions - with MTZ (5% *w*/w) and without MTZ (blank polymers) were manufactured. While PCL is a hydrophobic polymer, MTZ is a water-soluble drug (Labet and Thielemans, 2009; Sweetman, 2009), it was therefore a challenge to incorporate MTZ in the PCL polymer mixture. Accordingly, the reduction of MTZ particle size played an important role to allow more homogenous drug-polymer mixture that could be extruded through the 3D printer nozzle. The final particle size of the drug powder ranged from 2.11 and 6.51 μm (4.70 ± 1.61 μm, n = 12) (Fig. S1 in supporting information). The mixture of H-PCL and L-PCL was chosen based on the results of previous studies, which showed excellent extrusion properties using the 3D bioprinter (Domínguez-Robles et al., 2021a, 2021b). For instance, vascular grafts containing dipyridamole and aspirin were successfully 3D-printed using this polymer combination (60% of H-PCL and 40% of L-PCL) (Domínguez-Robles et al., 2021a, 2021b). Hence, the drug and polymer mixture was able to be continuously extruded, and the 3D-printed materials were solid and homogenous with desirable shape and size, as can be seen in Fig. 1A-B.

In addition, another mucoadhesive layer was successfully printed on the top of the vaginal disc containing MTZ using the same 3D bioprinter. The type of mucoadhesive polymer was an important consideration due to the hydrophobicity of PCL. Hydrophilic mucoadhesive polymer, such as chitosan, was not able to stick on the surface of the device (data not shown). Consequently, Gantrez™ AN-119 was chosen to be the most suitable mucoadhesive polymer as it is soluble in acetone. On the other hand, PCL is also soluble in acetone. As a result, the Gantrez™ AN-119 layer was able to be printed and affixed securely on to the surface of the PCL-based 3D-printed materials, as shown by using different imaging techniques (Fig. 1C-F). Light and scanning electron microscope images, as well as OCT images show how this mucoadhesive layer was printed and successfully attached to the PCL-based surface. Moreover, the OCT picture (Fig. 1E) is exhibiting the different thickness of both parts of the implants. While PCL-based part of the implant had a thickness which ranged from 0.4 to 0.65 mm, the thickness of the mucoadhesive layer (represented in both directions) ranged from 0.1 to 0.2 mm. Additionally, a SEM micrograph was used to show the top view of the mucoadhesive layer of the implants in more detail (Fig. 1F). This part of work also demonstrated the versatility of 3D bioprinter for the manufacture of different materials. A cartridge equipped with thermal and mechanical force controls was used to 3D-print PCL-based devices, while a different cartridge equipped with air pressure force (with no temperature) was used to 3D print the mucoadhesive layer.

3.2. Physicochemical characterisation

Several tests were performed to determine the properties of the 3D-

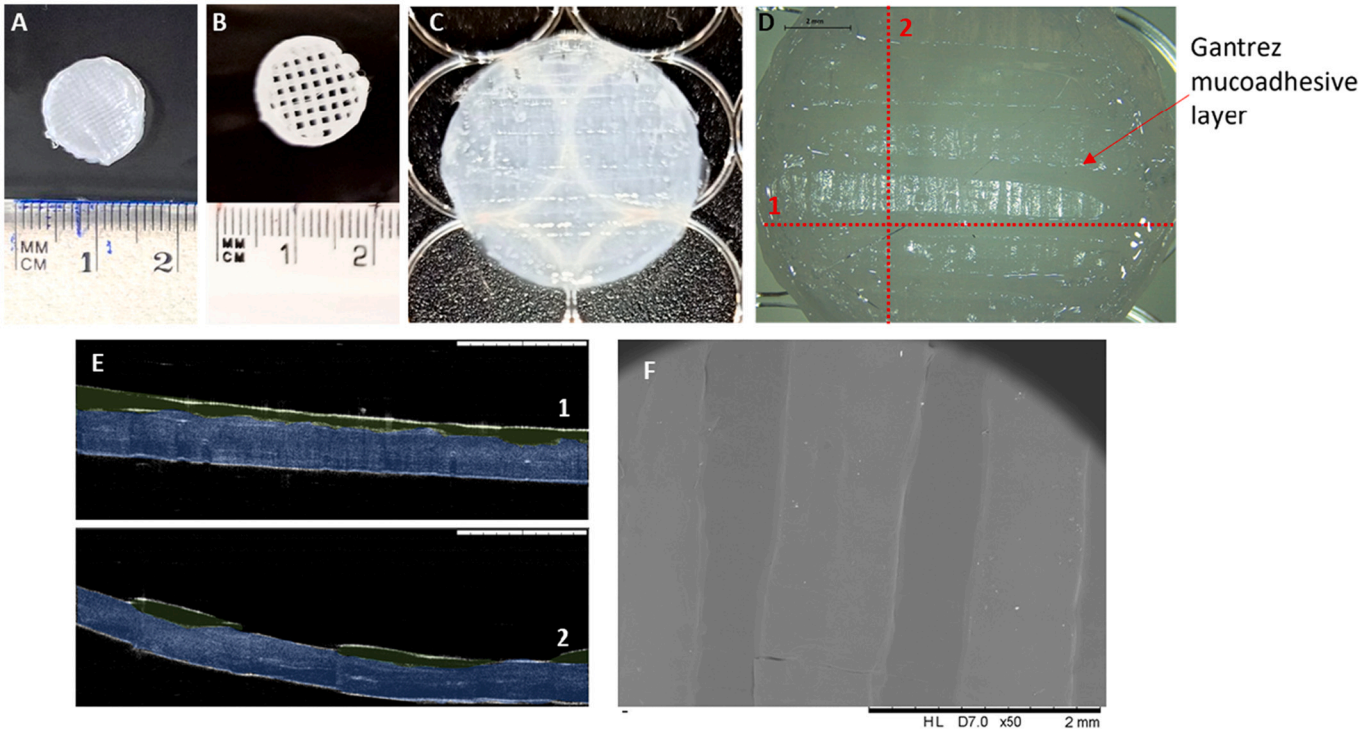

Fig. 1. Digital pictures of a MTZ-loaded disc (A) and mesh (B). Picture of a MTZ-loaded disc containing the mucoadhesive layer of Gantrez™-AN119 (C) and by using a magnification of 8× (D). OCT image of the 3D-printed intravaginal device showing the different thickness of both the PCL-based part (blue) and mucoadhesive layer (green) (represented in both directions: 1 and 2) (E). SEM image showing the top view of the mucoadhesive layer of the 3D-printed intravaginal device (F). (For interpretation of the references to colour in this figure legend, the reader is referred to the web version of this article.)

printed intravaginal devices, including surface analysis, thermal properties, FTIR and XRD analysis, and drug content analysis. The morphology of the surface of the MTZ-loaded 3D-printed devices was evaluated using SEM. Fig. 2 shows the surface of both MTZ-loaded discs and meshes. Moreover, the surface of the 3D-printed meshes containing no MTZ was also evaluated to compare with the MTZ-loaded ones. As expected, the surface of the 3D-printed meshes containing no drug was very smooth and quite homogeneous. These results are thus corroborating the successful mixing of both H-PCL and L-PCL by using the dual asymmetric centrifugal laboratory mixer system and the 3D printing process, as previously reported (Domínguez-Robles et al., 2021a, 2021b). Regardless the shape, it can be seen that MTZ was homogenously dispersed on the surface of the MTZ-loaded 3D-printed material. Additionally, the morphology of each formulation after the release studies was investigated and shown in the Section 3.3.

The thermal properties of the pure MTZ and H-PCL powders, as well as the 3D printed materials were analysed using both DSC and TGA. The results were shown in Fig. 3. A sharp endothermic peak at 162.37 °C indicated the melting point of the pure MTZ. However, this peak was not observed in the curves of the MTZ-loaded 3D printed materials. Interestingly, MTZ particles were found in SEM images dispersed over the surface of the meshes. Therefore, it can be inferred that the amount crystalline drug is too small to be detected using DSC. XRD analysis was performed to ascertain MTZ crystallinity. Another endothermic peak at 58 °C was found in both blank and drug-loaded 3D-printed materials. This peak represented the melting point of the PCL blend. It can be seen that this peak was not shifted after the addition of MTZ in the formulations. However, the melting point of these blank formulations (around 58 °C) was slightly lower compared to the one found at 61.36 °C for the pure high-molecular-weight PCL (H-PCL). Therefore, the addition of low-molecular-weight PCL (L-PCL) in the blank formulations has an effect lowering the melting temperature of these blank formulations, as has previously been reported (Stewart et al., 2020). The reduction of the melting temperature observed in the blank formulations can be supported by a reduction in crystallinity of the H-PCL/L-PCL blends. These results are in line with previous outcomes indicating that the crystallinity of PCL-based materials can be influenced by the content of L-PCL (Stewart et al., 2020, 2021).

On the other hand, based on the TGA results, it can be seen that the incorporation of L-PCL reduced the degradation temperature of the blank formulations. Related to the DSC analysis results, the increase of the amorphous part in the blank formulations required less energy to degrade the material, which led to the lower degradation temperature than H-PCL itself (Moseson et al., 2020). Additionally, compared to the

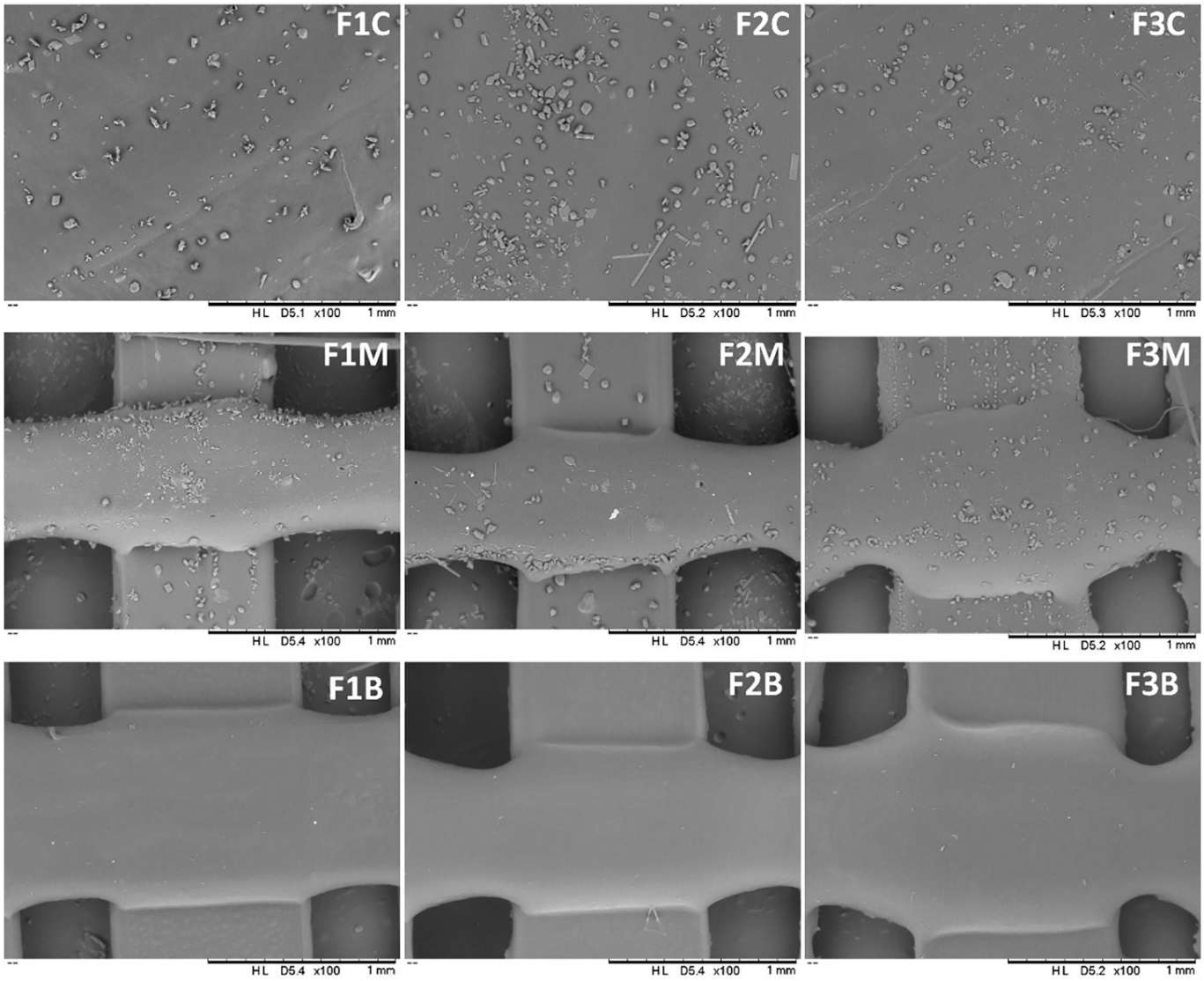

Fig. 2. SEM images of the MTZ-loaded vaginal discs (F1C, F2C, and F3C), MTZ-loaded vaginal meshes (F1M, F2M, and F3M), and blank formulations (F1B, F2B, and F3B).

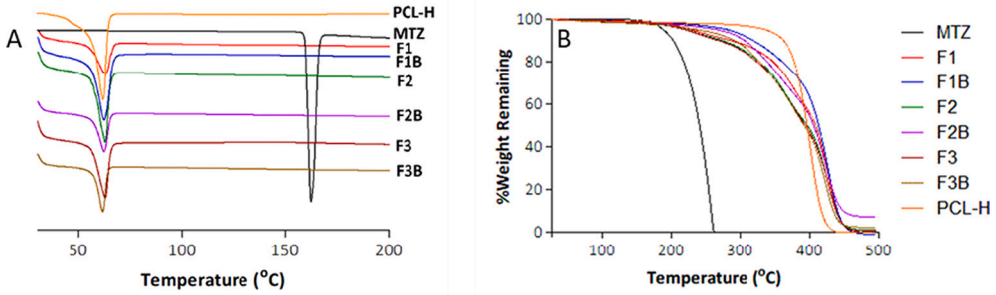

Fig. 3. The results of DSC (A) and TGA (B) analysis of pristine MTZ and H-PCL and all the 3D-printed formulations.

pure MTZ, which started to degrade at around 200 °C, the PCL-based devices, both blank and MTZ-loaded formulations, started to degrade at higher temperatures, of s over 250 °C. This suggests that PCL was able to enhance the degradation temperature of the formulations. These results were able to ensure that no degradation occurred during the 3D printing process as the temperature used (60 °C) was below the degradation temperature.

Chemical interaction of MTZ and other excipients was evaluated using FTIR. Fig. 4A presented the spectra of all the 3D-printed formulations, as well as the pure MTZ powder. Characteristic peaks of the pure MTZ were observed in all the spectra of the MTZ-loaded formulations. The peak at 3216 cm^{-1} was attributed to O—H stretching. Moreover, C═CH stretching vibration was appeared in the range of 3100–3000 cm^{-1}. A sharp peak at 1535 cm^{-1} indicated N═O stretching vibration and a strong peak for C-OH stretching vibration was observed at 1186 cm^{-1} (Nnamani and Okonkwo, 2017; Obaidat et al., 2022).

The crystallinity of MTZ was further investigated using XRD analysis. The diffractograms of the formulations and the pure MTZ are shown in Fig. 4B. It can be seen that the diffractogram of MTZ reflected its crystalline properties, which was in good agreement with the results of DSC measurement. Additionally, the diffractograms of the formulations containing MTZ showed the presence of MTZ peaks indicating that the drug crystals were dispersed within the polymer matrix as evidenced by SEM analysis. MTZ characteristic peaks at around 15 and 28° can be observed in F1, F2 and F3 formulations.

Table 2 presents the percentage of MTZ loaded in the intravaginal devices. The results showed that the MTZ concentration in the formulation ranged between 4.54 and 5.03% (*w*/w) with the recovery percentage of 90.74–100.68%. These results are therefore corroborating the previous outcomes, indicating that the loaded drug was homogeneously distributed in the 3D-printed materials.

Table 2
The results of drug content analysis in the PCL-based intravaginal devices.

Formulations	Drug content (%)	Recovery percentage (%)
F1	5.03 ± 0.14%	100.68 ± 2.87%
F2	4.54 ± 0.09%	90.74 ± 1.7%
F3	4.85 ± 0.08%	96.92 ± 1.57%

3.3. *In vitro release study*

The release profiles of both MTZ-loaded meshes and discs are presented in Fig. 5. Briefly, it was obvious that the discs were able to sustain the release of MTZ relatively longer than the meshes. The MTZ release from the meshes was obtained until day-9, while it took 14 days to completely release MTZ from the discs. Nevertheless, the majority of the drug was released in the first days, most likely due to hydrophilicity of MTZ (Biagi, 1982). Indeed, the amount of drug released from MTZ-loaded discs (F1 and F2) and F1 from MTZ-loaded meshes was significantly different until 72 h ($p < 0.05$), thus these formulations reached a plateau on the fourth day. Moreover, the amount of MTZ released from the F3 of the MTZ-loaded discs was significantly different until the ninth day ($p < 0.05$). However, no significant differences were found in the MTZ-loaded meshes (F2 and F3) after 24 h ($p > 0.05$). These results indicated that the shape of the devices did influence the release behavior of MTZ. The meshes possessed a larger surface area compared to the flat discs. Accordingly, in the case of MTZ meshes, a larger area was in contact with the release media, resulting in faster release of MTZ (Khaled et al., 2018a; Kyobula et al., 2017; Martinez et al., 2018).

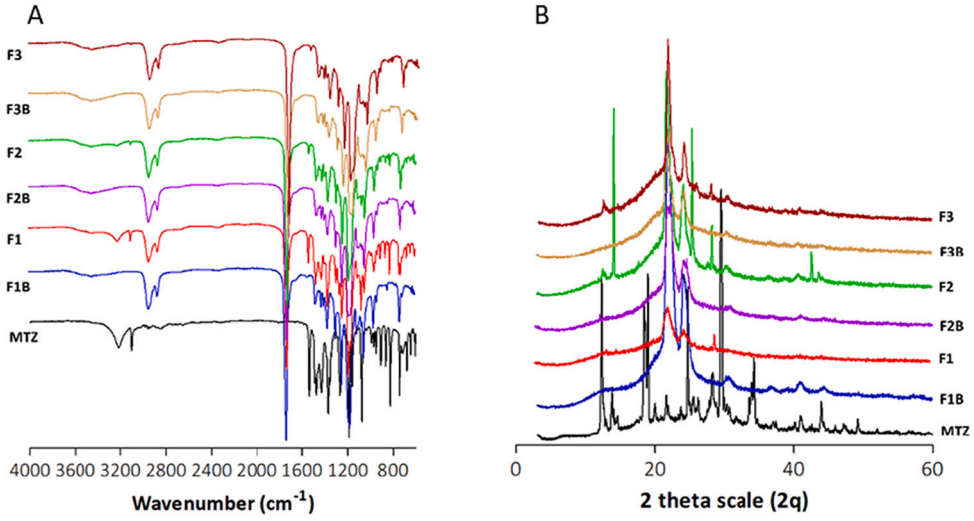

Fig. 4. The results of FTIR analysis (A) and XRD analysis (B) of MTZ and the devices' formulations.

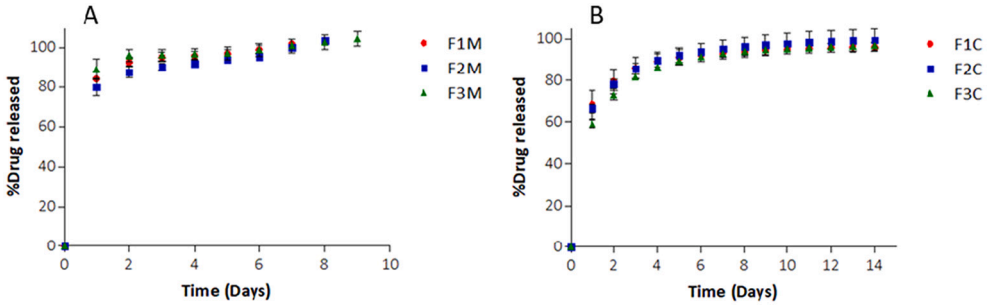

Fig. 5. The release profiles of MTZ-loaded vaginal meshes (A) and MTZ-loaded vaginal discs (B).

In terms of the formulation compositions, based on the similarity and different factors analysis, no significant difference was observed among all formulations (Table 3). Therefore, the different ratio of H-PCL and L-PCL in both designs (meshes and discs) did not influence their respective drug release profiles. This may be caused by the properties of MTZ itself. The hydrophilicity of MTZ prevented its dissolution in the mixture of PCL, as PCL is known for its hydrophobicity. As previously observed in the SEM images (Fig. 2), MTZ was dispersed on the surface of the devices. Moreover, the devices were only composed of two MTZ-containing layers, together with the additional mucoadhesive layer. Therefore, both the MTZ hydrophilicity and the thickness of the performed devices may be influencing their drug release behavior (Biagi, 1982; Obeid et al., 2021). Accordingly, a more sustained release could be achieved by increasing the thickness of the devices, thus increasing the treatment duration. Besides the thickness, the diameter and probably the drug dose can be increased (Domínguez-Robles et al., 2021a), thus the required daily dose could be achieved. Furthermore, Fig. 6 presents the images of the devices at the end of the release study. It was clear that no MTZ was observed on the surface of the devices indicating that MTZ was completely released from the meshes and discs to the release media after 9 and 14 days, respectively.

3.4. Antimicrobial activity test

A disk diffusion experiment was performed to evaluate the antimicrobial activity of the MTZ-eluting 3D-printed materials. A representative picture of the obtained results by the disk diffusion test is displayed in the Fig. 7. As expected, the MTZ-eluting 3D-printed discs showed a clear zone of inhibition in both *G. vaginalis* plates with the diameter of 19.0 ± 1.3 mm ($n = 3$). Moreover, the 3D-printed discs without MTZ did not inhibit bacterial growth, confirming that PCL possessed no antimicrobial effect. These results show the *in vitro* efficacy of the performed 3D-printed dosage forms, indicating the efficacy of MTZ was able to be maintained in the formulations. Accordingly, these devices might represent a valuable alternative to the marketed cream-based or oral dosage forms used for the treatment of BV. Currently available treatments for BV require multiple administrations; however, the intravaginal devices in this work provide sustained release of MTZ, negating repeated dosing. Accordingly, these vaginal devices are likely to increase patient compliance, which may contribute to the success of the BV treatment.

Table 3
The results of similarities and different factors analysis of the release profiles of MTZ-loaded vaginal devices formulations.

Curve 1	Curve 2	f_1	f_2
F1M	F2M	2.36%	79.59
F1M	F3M	2.28%	72.36
F2M	F3M	3.58%	71.53
F1C	F2C	3.53%	66.37
F1C	F3C	1.71%	80.36
F2C	F3C	4.50%	63.84

3.5. Mucoadhesion test

The mucoadhesion test was performed to assess the mucoadhesive properties of the 3D-printed discs with an additional mucoadhesive layer of Gantrez™-AN119. The versatility of the 3D bioprinter was explored by using two different material cartridges to 3D print the PCL-based intravaginal devices containing the Gantrez™-AN119 mucoadhesive layer. The Gantrez™ polymers have been extensively used to manufacture mucoadhesive drug delivery systems (Andrews et al., 2009; Mc Crudden et al., 2019). The force required to separate the 3D-printed devices containing the mucoadhesive layer from a partially hydrated mucin disk were evaluated and presented in Fig. 7B. The 3D-printed devices containing the mucoadhesive layer exhibited higher mucoadhesive bond strength (2.6 ± 1.1 N) than the control formulations (0.5 ± 0.3), those without the mucoadhesive layer ($p < 0.05$). The values of the adhesion forces of the 3D-printed devices containing the mucoadhesive layer, exceed those previously reported for other vaginal drug delivery systems, including the values found for the commercially available Replens formulation (⟨1N) (Andrews et al., 2009; Hassan et al., 2018). Moreover, the highest adhesion force values found in this study are in agreement with those reported in the literature for rilpivirine-loaded dissolving microarray patches (MAPs) for intravaginal delivery (2.9 ± 0.3 N) (Mc Crudden et al., 2019). Therefore, the retention of these PCL-based intravaginal devices can be enhanced using mucoadhesive polymers, such as Gantrez™-AN119. The adhesion forces are essential to maximize residency and, thus, clinical performance and patient compliance.

4. Conclusions

MTZ-loaded intravaginal devices were successfully prepared using SSE 3D printing technology. In this study, H-PCL was mixed with L-PCLPCL to obtain the desirable properties to be printed using the 3D bioprinter in two different shapes, namely meshes and discs. It was found that the surface of the 3D-printed samples containing no drug were quite homogeneous indicating that both H-PCL and L-PCL were successfully mixed. Moreover, MTZ was homogenously dispersed on the MTZ-loaded 3D-printed material. Following *in vitro* release studies, the release of MTZ from the meshes was faster compared to the disc form, as expected due to the higher surface area of the meshes. Moreover, an additional layer of Gantrez™-AN119 using the same 3D bioprinter was included in the PCL-based intravaginal devices to provide mucoadhesive properties, thus, showing the versatility of the 3D printing technology as a manufacturing technique for the production of drug-loaded dosage forms. The values of the adhesion forces reported in this study for the 3D-printed devices containing the mucoadhesive layer were higher than those previously shown for other vaginal drug delivery systems. Accordingly, the residence time can be enhanced and, thus, the clinical performance of these devices. The microbiological assay also exhibited that MTZ-loaded discs were able to inhibit the growth of *Gardnerella vaginalis*. Therefore, the present work shows the potential of the 3D-printed PCL-based intravaginal devices as an alternative treatment for

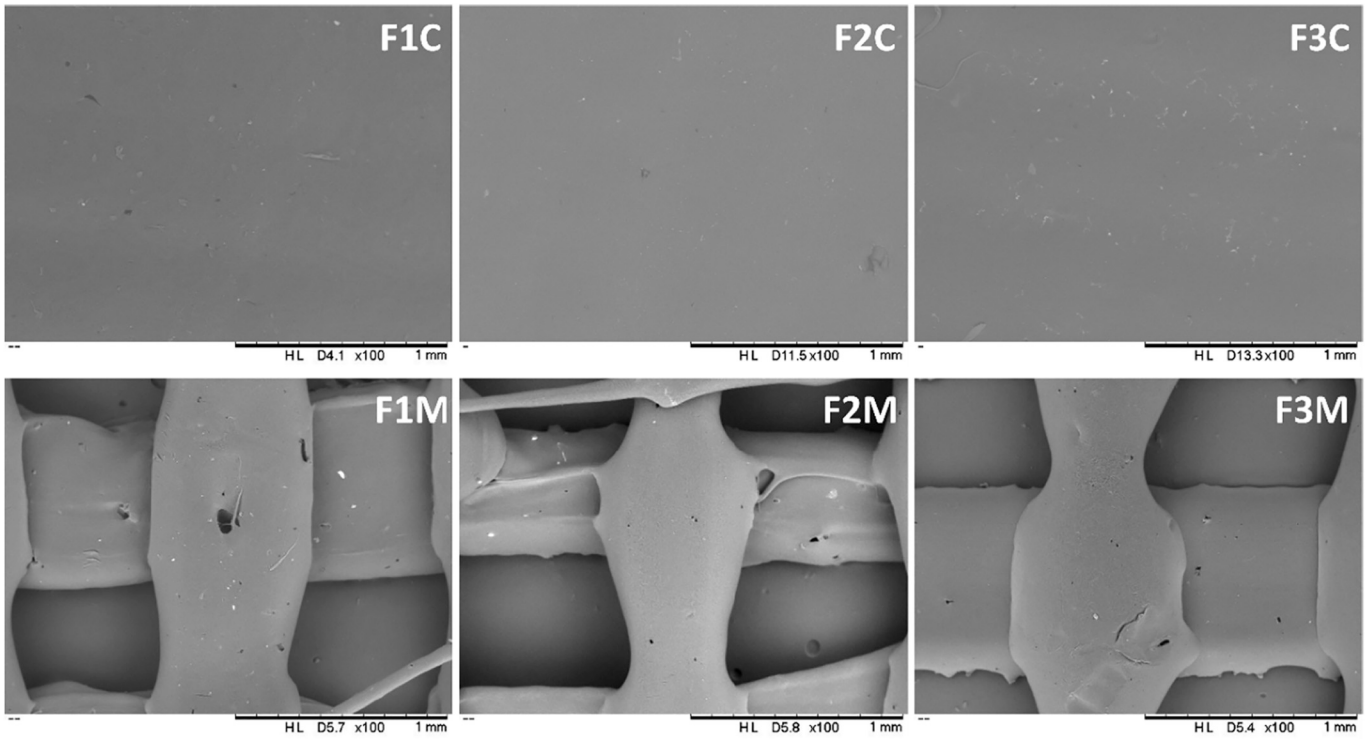

Fig. 6. SEM images of MTZ-loaded vaginal discs (F1C, F2C, and F3C) and MTZ-loaded vaginal meshes (F1M, F2M, and F3M) after the release study.

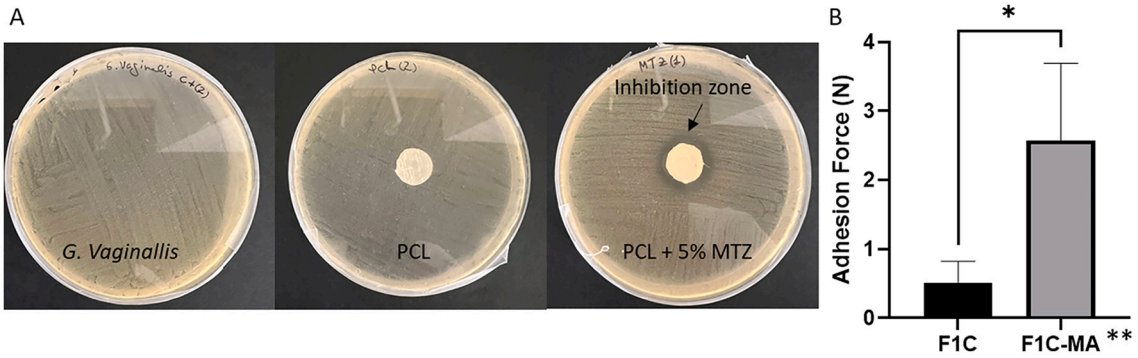

Fig. 7. A representative picture showing the zone of inhibition obtained for *G. vaginalis* in BHI agar plates (A). A graph presenting the force required to detach F1C-MA from the mucin tablet (B). F1C-MA** means MTZ-loaded discs of F1 containing the mucoadhesive layer.

BV. Moving forward, *in vivo* studies are required to assess the efficacy of these devices using suitable animal models.

Declaration of Competing Interest

None.

Data availability

The authors are unable or have chosen not to specify which data has been used.

Acknowledgements

This work was financially supported by the Wellcome Trust (UNS40040) and the Queen's University Belfast CITI-GENS project funded by the European Union's Horizon 2020 under the Marie Skłodowska-Curie grant agreement [No 945231].

Appendix A. Supplementary data

Supplementary data to this article can be found online at https://doi.org/10.1016/j.ijpx.2022.100142.

References

Ali, A., Ahmad, U., Akhtar, J., 2020. 3D Printing in Pharmaceutical Sector: An Overview, in: Pharmaceutical Formulation Design - Recent Practices. IntechOpen. https://doi.org/10.5772/intechopen.90738.

Andrews, G.P., Donnelly, L., Jones, D.S., Curran, R.M., Morrow, R.J., Woolfson, A.D., Malcolm, R.K., 2009. Characterization of the rheological, mucoadhesive, and drug release properties of highly structured gel platforms for intravaginal drug delivery. Biomacromolecules 10, 2427–2435. https://doi.org/10.1021/bm9003332.

Anjani, Q.K., Sabri, A.H. Bin, Domínguez-Robles, J., Moreno-Castellanos, N., Utomo, E., Wardoyo, L.A.H., Larrañeta, E., Donnelly, R.F., 2022. Metronidazole nanosuspension loaded dissolving microarray patches: an engineered composite pharmaceutical system for the treatment of skin and soft tissue infection. Biomater. Adv. 140, 213073 https://doi.org/10.1016/j.bioadv.2022.213073.

Arany, P., Papp, I., Zichar, M., Regdon, G., Béres, M., Szalóki, M., Kovács, R., Fehér, P., Ujhelyi, Z., Vecsernyés, M., Bácskay, I., 2021. Manufacturing and examination of vaginal drug delivery system by FDM 3D printing. Pharmaceutics 13, 1714. https://doi.org/10.3390/pharmaceutics13101714.

Awad, A., Fina, F., Trenfield, S., Patel, P., Goyanes, A., Gaisford, S., Basit, A., 2019. 3D printed pellets (miniprintlets): a novel, multi-drug, controlled release platform technology. Pharmaceutics 11, 148. https://doi.org/10.3390/pharmaceutics11040148.

Biagi, G.L., 1982. The pharmacology and toxicology of 5-nitroimidazoles. In: Nitroimidazoles. Springer US, Boston, MA, pp. 1–7. https://doi.org/10.1007/978-1-4684-4151-2_1.

Chavoustie, S.E., Jacobs, M., Reisman, H.A., Waldbaum, A.S., Levy, S.F., Hillier, S.L., Nyirjesy, P., 2015. Metronidazole vaginal gel 1.3% in the treatment of bacterial vaginosis. J. Low. Genit. Tract Dis. 19, 129–134. https://doi.org/10.1097/LGT.0000000000000062.

Diaz, D.A., Colgan, S.T., Langer, C.S., Bandi, N.T., Likar, M.D., Van Alstine, L., 2016. Dissolution similarity requirements: how similar or dissimilar are the global regulatory expectations? AAPS J. 18, 15–22. https://doi.org/10.1208/s12248-015-9830-9.

Dominguez-Robles, J., Martin, N.K., Fong, M.L., Stewart, S.A., Irwin, N.J., Rial-Hermida, M.I., Donnelly, R.F., Larraneta, E., 2019. Antioxidant PLA composites containing lignin for 3D printing applications: a potential material for healthcare applications. Pharmaceutics 11, 165. https://doi.org/10.3390/pharmaceutics11040165.

Domínguez-Robles, J., Mancinelli, C., Mancuso, E., García-Romero, I., Gilmore, B.F.B.F., Casettari, L., Larrañeta, E., Lamprou, D.A.D.A., 2020. 3D printing of drug-loaded thermoplastic polyurethane meshes: a potential material for soft tissue reinforcement in vaginal surgery. Pharmaceutics 12, 63. https://doi.org/10.3390/pharmaceutics12010063.

Domínguez-Robles, J., Diaz-Gomez, L., Utomo, E., Shen, T., Picco, C.J., Alvarez-Lorenzo, C., Concheiro, A., Donnelly, R.F., Larrañeta, E., 2021a. Use of 3D printing for the development of biodegradable antiplatelet materials for cardiovascular applications. Pharmaceuticals 14, 921. https://doi.org/10.3390/ph14090921.

Domínguez-Robles, J., Shen, T., Cornelius, V.A., Corduas, F., Mancuso, E., Donnelly, R.F., Margariti, A., Lamprou, D.A., Larrañeta, E., 2021b. Development of drug loaded cardiovascular prosthesis for thrombosis prevention using 3D printing. Mater. Sci. Eng. C 129, 112375. https://doi.org/10.1016/j.msec.2021.112375.

Domínguez-Robles, J., Utomo, E., Cornelius, V.A., Anjani, Q.K., Korelidou, A., Gonzalez, Z., Donnelly, R.F., Margariti, A., Delgado-Aguilar, M., Tarrés, Q., Larrañeta, E., 2022. TPU-based antiplatelet cardiovascular prostheses prepared using fused deposition modelling. Mater. Des. 220, 110837 https://doi.org/10.1016/j.matdes.2022.110837.

El Aita, I., Breitkreutz, J., Quodbach, J., 2020. Investigation of semi-solid formulations for 3D printing of drugs after prolonged storage to mimic real-life applications. Eur. J. Pharm. Sci. 146, 105266 https://doi.org/10.1016/j.ejps.2020.105266.

Farmer, Z.-L., Domínguez-Robles, J., Mancinelli, C., Larrañeta, E., Lamprou, D.A., 2020. Urogynecological surgical mesh implants: new trends in materials, manufacturing and therapeutic approaches. Int. J. Pharmaceut. 585, 119512 https://doi.org/10.1016/j.ijpharm.2020.119512.

Farmer, Z.-L., Utomo, E., Domínguez-Robles, J., Mancinelli, C., Mathew, E., Larrañeta, E., Lamprou, D.A., 2021. 3D printed estradiol-eluting urogynecological mesh implants: Influence of material and mesh geometry on their mechanical properties. Int. J. Pharmaceut. 593, 120145 https://doi.org/10.1016/j.ijpharm.2020.120145.

Goje, O., Shay, E.O., Markwei, M., Padmanabhan, R., Eng, C., 2021. The effect of oral metronidazole on the vaginal microbiome of patients with recurrent bacterial vaginosis: a pilot investigational study. Hum. Microbiome J. 20, 100081 https://doi.org/10.1016/j.humic.2021.100081.

Goyanes, A., Chang, H., Sedough, D., Hatton, G.B., Wang, J., Buanz, A., Gaisford, S., Basit, A.W., 2015. Fabrication of controlled-release budesonide tablets via desktop (FDM) 3D printing. Int. J. Pharmaceut. 496, 414–420. https://doi.org/10.1016/j.ijpharm.2015.10.039.

Hanson, J.M., McGregor, J.A., Hillier, S.L., Eschenbach, D.A., Kreutner, A.K., Galask, R. P., Martens, M., 2001. Metronidazole for bacterial vaginosis: a comparison of vaginal gel vs. oral therapy. Obstet. Gynecol. Surv. 56, 145–146. https://doi.org/10.1097/00006254-200103000-00014.

Hassan, A.S., Soliman, G.M., Ali, M.F., El-Mahdy, M.M., El-Gindy, G.E.-D.A., 2018. Mucoadhesive tablets for the vaginal delivery of progesterone: in vitro evaluation and pharmacokinetics/pharmacodynamics in female rabbits. Drug Dev. Ind. Pharm. 44, 224–232. https://doi.org/10.1080/03639045.2017.1386203.

Herman, T.F., Santos, C., 2022. First Pass Effect [WWW Document]. URL. https://www.statpearls.com/ArticleLibrary/viewarticle/21783.

Irache, J., Huici, M., Konecny, M., Espuelas, S., Campanero, M., Arbos, P., 2005. Bioadhesive properties of Gantrez nanoparticles. Molecules 10, 126–145. https://doi.org/10.3390/10010126.

Jones, A., 2019. Bacterial vaginosis: a review of treatment, recurrence, and disparities. J. Nurse Pract. 15, 420–423. https://doi.org/10.1016/j.nurpra.2019.03.010.

Khaled, S.A., Alexander, M.R., Irvine, D.J., Wildman, R.D., Wallace, M.J., Sharpe, S., Yoo, J., Roberts, C.J., 2018a. Extrusion 3D printing of paracetamol tablets from a single formulation with tunable release profiles through control of tablet geometry. AAPS PharmSciTech 19, 3403–3413. https://doi.org/10.1208/s12249-018-1107-z.

Khaled, S.A., Alexander, M.R., Wildman, R.D., Wallace, M.J., Sharpe, S., Yoo, J., Roberts, C.J., 2018b. 3D extrusion printing of high drug loading immediate release paracetamol tablets. Int. J. Pharmaceut. 538, 223–230. https://doi.org/10.1016/j.ijpharm.2018.01.024.

Korelidou, A., Domínguez-Robles, J., Magill, E.R., Eleftheriadou, M., Cornelius, V.A., Donnelly, R.F., Margariti, A., Larrañeta, E., 2022. 3D-printed reservoir-type implants containing poly(lactic acid)/poly(caprolactone) porous membranes for sustained drug delivery. Biomater. Adv. 139, 213024 https://doi.org/10.1016/j.bioadv.2022.213024.

Kyobula, M., Adedeji, A., Alexander, M.R., Saleh, E., Wildman, R., Ashcroft, I., Gellert, P. R., Roberts, C.J., 2017. 3D inkjet printing of tablets exploiting bespoke complex geometries for controlled and tuneable drug release. J. Control. Release 261, 207–215. https://doi.org/10.1016/j.jconrel.2017.06.025.

Labet, M., Thielemans, W., 2009. Synthesis of polycaprolactone: a review. Chem. Soc. Rev. 38, 3484. https://doi.org/10.1039/b820162p.

Larrañeta, E., Martínez-Ohárriz, C., Vélaz, I., Zornoza, A., Machín, R., Isasi, J.R., 2014. In vitro release from reverse poloxamine/α-cyclodextrin matrices: modelling and comparison of dissolution profiles. J. Pharm. Sci. 103, 197–206. https://doi.org/10.1002/jps.23774.

Löfmark, S., Edlund, C., Nord, C.E., 2010. Metronidazole is still the drug of choice for treatment of anaerobic infections. Clin. Infect. Dis. 50, S16–S23. https://doi.org/10.1086/647939.

Martinez, P.R., Goyanes, A., Basit, A.W., Gaisford, S., 2018. Influence of geometry on the drug release profiles of stereolithographic (SLA) 3D-printed tablets. AAPS PharmSciTech 19, 3355–3361. https://doi.org/10.1208/s12249-018-1075-3.

Mathew, E., Domí-nguez-Robles, J., Stewart, S.A., Mancuso, E., O'Donnell, K., Larrañeta, E., Lamprou, D.A., 2019. Fused deposition modeling as an effective tool for anti-infective dialysis catheter fabrication. ACS Biomater. Sci. Eng. 5, 6300–6310. https://doi.org/10.1021/acsbiomaterials.9b01185.

Mc Crudden, M.T.C., Larrañeta, E., Clark, A., Jarrahian, C., Rein-Weston, A., Creelman, B., Moyo, Y., Lachau-Durand, S., Niemeijer, N., Williams, P., McCarthy, H. O., Zehrung, D., Donnelly, R.F., 2019. Design, formulation, and evaluation of novel dissolving microarray patches containing rilpivirine for intravaginal delivery. Adv. Healthc. Mater. 8, 1801510. https://doi.org/10.1002/adhm.201801510.

Mitchell, C.M., Hitti, J.E., Agnew, K.J., Fredricks, D.N., 2009. Comparison of oral and vaginal metronidazole for treatment of bacterial vaginosis in pregnancy: impact on fastidious bacteria. BMC Infect. Dis. 9, 89. https://doi.org/10.1186/1471-2334-9-89.

Mohammed, A.A., Algahtani, M.S., Ahmad, M.Z., Ahmad, J., 2021. Optimization of semisolid extrusion (pressure-assisted microsyringe)-based 3D printing process for advanced drug delivery application. Ann. 3D Print. Med. 2, 100008 https://doi.org/10.1016/j.stlm.2021.100008.

Morrill, S., Gilbert, N.M., Lewis, A.L., 2020. Gardnerella vaginalis as a cause of bacterial vaginosis: appraisal of the evidence from in vivo models. Front. Cell. Infect. Microbiol. 10 https://doi.org/10.3389/fcimb.2020.00168.

Moseson, D.E., Jordan, M.A., Shah, D.D., Corum, I.D., Alvarenga Jr., B.R., Taylor, L.S., 2020. Application and limitations of thermogravimetric analysis to delineate the hot melt extrusion chemical stability processing window. Int. J. Pharmaceut. 590, 119916 https://doi.org/10.1016/j.ijpharm.2020.119916.

Muselík, J., Komersová, A., Kubová, K., Matzick, K., Skalická, B., 2021. A critical overview of FDA and EMA statistical methods to compare in vitro drug dissolution profiles of pharmaceutical products. Pharmaceutics 13, 1703. https://doi.org/10.3390/pharmaceutics13101703.

Muzny, C.A., Kardas, P., 2020. A narrative review of current challenges in the diagnosis and management of bacterial vaginosis. Sex. Transm. Dis. 47, 441–446. https://doi.org/10.1097/OLQ.0000000000001178.

Nnamani, N.D., Okonkwo, T.J.N., 2017. Optimization of metronidazole tablet formulation using Manihot utilissima starch and a combination of processing techniques. Futur. J. Pharm. Sci. 3, 65–70. https://doi.org/10.1016/j.fjps.2017.03.002.

Obaidat, R., Abu Kwiak, A.D., Hamed, R., 2022. Development of combined therapy of metronidazole and ibuprofen using in situ microgels for the treatment of periodontitis. J. Drug Deliv. Sci. Technol. 71, 103314 https://doi.org/10.1016/j.jddst.2022.103314.

Obeid, S., Madžarević, M., Ibrić, S., 2021. Tailoring amlodipine release from 3D printed tablets: Influence of infill patterns and wall thickness. Int. J. Pharmaceut. 610, 121261 https://doi.org/10.1016/j.ijpharm.2021.121261.

Patil, P., Datir, S., Saudagar, R., 2019. A review on topical gels as drug delivery system. J. Drug Deliv. Ther. 9, 661–668.

Rastogi, R., Su, J., Mahalingam, A., Clark, J., Sung, S., Hope, T., Kiser, P.F., 2016. Engineering and characterization of simplified vaginal and seminal fluid simulants. Contraception 93, 337–346. https://doi.org/10.1016/j.contraception.2015.11.008.

Redelinghuys, M.J., Geldenhuys, J., Jung, H., Kock, M.M., 2020. Bacterial vaginosis: current diagnostic avenues and future opportunities. Front. Cell. Infect. Microbiol. 10 https://doi.org/10.3389/fcimb.2020.00354.

Robles-Martinez, P., Xu, X., Trenfield, S.J., Awad, A., Goyanes, A., Telford, R., Basit, A. W., Gaisford, S., 2019. 3D printing of a multi-layered polypill containing six drugs using a novel stereolithographic method. Pharmaceutics 11, 274. https://doi.org/10.3390/pharmaceutics11060274.

Seoane-Viaño, I., Januskaite, P., Alvarez-Lorenzo, C., Basit, A.W., Goyanes, A., 2021. Semi-solid extrusion 3D printing in drug delivery and biomedicine: personalised solutions for healthcare challenges. J. Control. Release 332, 367–389. https://doi.org/10.1016/j.jconrel.2021.02.027.

Stewart, S.A., Domínguez-Robles, J., Donnelly, R.F., Larrañeta, E., 2018. Implantable polymeric drug delivery devices: classification, manufacture, materials, and clinical applications. Polymers (Basel) 10, 1379. https://doi.org/10.3390/polym10121379.

Stewart, S.A., Domínguez-Robles, J., McIlorum, V.J., Gonzalez, Z., Utomo, E., Mancuso, E., Lamprou, D.A., Donnelly, R.F., Larrañeta, E., 2020. Poly(caprolactone)-based coatings on 3D-printed biodegradable implants: a novel strategy to prolong delivery of hydrophilic drugs. Mol. Pharm. 17, 3487–3500. https://doi.org/10.1021/acs.molpharmaceut.0c00515.

Stewart, S.A., Domínguez-Robles, J., Utomo, E., Picco, C.J., Corduas, F., Mancuso, E., Amir, M.N., Bahar, M.A., Sumarheni, S., Donnelly, R.F., Permana, A.D., Larrañeta, E., 2021. Poly(caprolactone)-based subcutaneous implant for sustained

delivery of levothyroxine. Int. J. Pharmaceut. 607, 121011 https://doi.org/10.1016/j.ijpharm.2021.121011.
Sweetman, S.C., 2009. Martindale: The Complete Drug Reference, 36th ed. Pharmaceutical Press, London.
Trenfield, S.J., Awad, A., Goyanes, A., Gaisford, S., Basit, A.W., 2018. 3D printing pharmaceuticals: drug development to frontline care. Trends Pharmacol. Sci. 39, 440–451. https://doi.org/10.1016/j.tips.2018.02.006.
Utomo, E., Domínguez-Robles, J., Moreno-Castellanos, N., Stewart, S.A., Picco, C.J., Anjani, Q.K., Simón, J.A., Peñuelas, I., Donnelly, R.F., Larrañeta, E., 2022. Development of intranasal implantable devices for schizophrenia treatment. Int. J. Pharmaceut. 624, 122061 https://doi.org/10.1016/j.ijpharm.2022.122061.
Verwijs, M.C., Agaba, S.K., Darby, A.C., van de Wijgert, J.H.H.M., 2020. Impact of oral metronidazole treatment on the vaginal microbiota and correlates of treatment failure. Am. J. Obstet. Gynecol. 222, 157.e1–157.e13. https://doi.org/10.1016/j.ajog.2019.08.008.
Yan, T.-T., Lv, Z.-F., Tian, P., Lin, M.-M., Lin, W., Huang, S.-Y., Chen, Y.-Z., 2020. Semi-solid extrusion 3D printing ODFs: an individual drug delivery system for small scale pharmacy. Drug Dev. Ind. Pharm. 46, 531–538. https://doi.org/10.1080/03639045.2020.1734018.